



## OPEN Root cause analysis and evaluation of corrective actions for discharge boom suspension failure in bucket wheel excavator

Włodzimierz Dudziński<sup>1</sup>, Piotr Odyjas<sup>2</sup>, Maciej Olejnik<sup>2</sup>, Przemysław Moczko<sup>2</sup>, Damian Pietrusiak<sup>2</sup> & Jędrzej Więckowski<sup>2</sup>✉

The article analyzes the failure of a bucket wheel excavator's discharge boom suspension. The failure caused significant operational disruption and financial losses. The study includes metallographic tests and FEM analysis of the damaged axle, revealing a fatigue fracture due to inappropriate material microstructure and a structural notch. The fracture led to the boom falling, damaging the excavator and conveyor. Corrective actions involved redesigning the axle and using suitable materials, verified through extensive testing, to enhance durability and prevent future failures, ensuring safer operation.

**Keywords** Bucket wheel excavator, Discharge boom, Fracture, Redesign

The purpose of the text below is to describe the causes of failure of a heavy industry machine. Machines of this type are usually complex structures created by a team of engineers. The safety of their operation is usually dependent on many factors. Usually, it is impossible to determine which of them are critical from the point of view of the global safety of a technical facility. The same applies to the machine discussed in the article. In the literature, many papers have been devoted to the root causes analysis of the occurrence of operational failures<sup>1-9</sup>. The technical object described in the article, which is bucket wheel excavator, belongs to the group of material handling machines and is used in open-pit mines, stockyards etc. Machines in this group are characterized by the fact that they are mainly produced in series of a few copies or as single machine. In addition, these are machines of considerable dimensions, the deadweight of which can reach several thousand tons. For this reason, errors in design, manufacturing and construction materials quality can significantly increase the likelihood of failures resulting from operation. Examples of machines from this group are shown in the Figs. 1 and 2.

The cases of damage to the machines described in the article are already known in the literature on the subject. Due to their complex structure and numerous mechanisms, the causes of their failure vary. Thematically similar work was described in 2014<sup>10</sup>. The mentioned work also applies to the discharge boom of the bucket wheel excavator. It describes the dynamic properties of the described part of the machine. On the basis of the FEM analysis, the research team identified unmanaged dynamic phenomena resulting from the structure of the carrying structure. Subsequently, design changes were proposed to improve the dynamic properties of the boom. They concerned the redesign of the discharge boom ties. From the point of view of the operational safety of the technical object described in the paper, the supporting elements are crucial<sup>11-13</sup>. In 2012, a paper describing the failures of tie rods of bucket wheel boom was also created<sup>14</sup>. As a result of cracks in the tie rods structure, discontinuities in the construction occurred. This caused the fall of the bucket wheel boom itself and the subsequent loss of stability by the entire machine. The cause of the failure, according to the information in the article, was "failure was a consequence of a brittle fracture by cleavage. The crack followed the heat-affected zone of a welded joint connecting a rectangular hollow section, member and a plate flange"<sup>14</sup>. The machines described in the article are also exposed to the formation of fatigue cracks, as in<sup>15,16</sup>. In the case of technical objects of such large dimensions, loss of stability is also a major threat; the effects of such an event are described in<sup>17</sup>.

The operational hazards, except of regular operational loads, of this type of machinery depend to a large extent on its use and place of operation. Machines used for material handling are mainly exposed to weather factors, lumps of transported materials, collisions with other technical objects, and wear and tear. In the case of mining machines, there are risks associated with mining, such as landslides, non-workable inclusions,

<sup>1</sup>The Witelon Collegium State University, Sejnowa 5A, 59-220 Legnica, Poland. <sup>2</sup>Wrocław University of Science and Technology, 27 Wybrzeże Stanisława Wyspiańskiego st., 50-370 Wrocław, Poland. ✉email: Jędrzej.wieckowski@pwr.edu.pl



**Fig. 1.** Bucket Wheel Reclaimer LZKS 125.16.



**Fig. 2.** Bucket wheel excavator KWK 1200 M.

etc.<sup>18</sup>. Wear and tear can be manifested by fatigue cracks that can occur in the structural nodes or components connecting individual parts of the machine. The second case is described in this article. Fatigue cracks are a big problem in these types of facilities for two main reasons. The first is the expected long service life<sup>19,20</sup>, often exceeding 30 years. The second is that some standards do not include a fatigue case<sup>21</sup> in the design calculation or this case is not properly described. As the many years of experience of the research team shows, this is an erroneous assumption<sup>22</sup>. For such large objects, this can lead to failures or even disasters. In 2007, a paper by Prof. Dudek was written on mining machinery disasters in Poland<sup>23</sup>. He describes in detail the consequences and causes of their occurrence. From reading this book, it can be concluded that the machines described in the article are complex technical objects, and the causes of their failure have various causes. These include, among others: material fatigue, errors in operation, material defects and design errors.

The objective of this article is to determine the causes of the failure, which is described in the next chapter. First, an analysis of the incident and the situation in which it occurred was carried out. Subsequently, detailed examinations of the damaged element were carried out. The aim of the investigation was to answer whether the cause of the failure was a material defect or a construction error. The main objective is to make changes to the design of the machine that will ensure continued safe operation.

### Description of failure and consequences

The case described in the article concerns damage to a component of a bucket wheel excavator, which in this case cooperated with self-propelled conveyor. Figure 3 shows the position of two machines relative to each other during normal operation. This bucket wheel excavator is used on site of operation to work with hard-mineable deposits. It was also designed for this purpose, and therefore it is characterized by a compact design. The failure in the presented case concerns the axle to which a luffing hydraulic cylinder (Fig. 4), controlling boom's position, is attached. This is one of the pivot points of the discharge boom relative to the rest of the excavator. This makes it possible to rotate within the range of  $-9.1^\circ$  do  $+9.8^\circ$ . This range of motion allows the excavator to work with a belt conveyor or with a self-propelled belt conveyor.

The boom suspension in the area of the axis connecting it with the rest of the machine's structure was damaged. It occurred in the form of a crack in the cross-section that prevented the axle from sliding out of the socket. Figure 5 shows a view of the axle immediately after a failure. Figure 6 presents a technical drawing of the axle with marked cross section that was cut during failure.

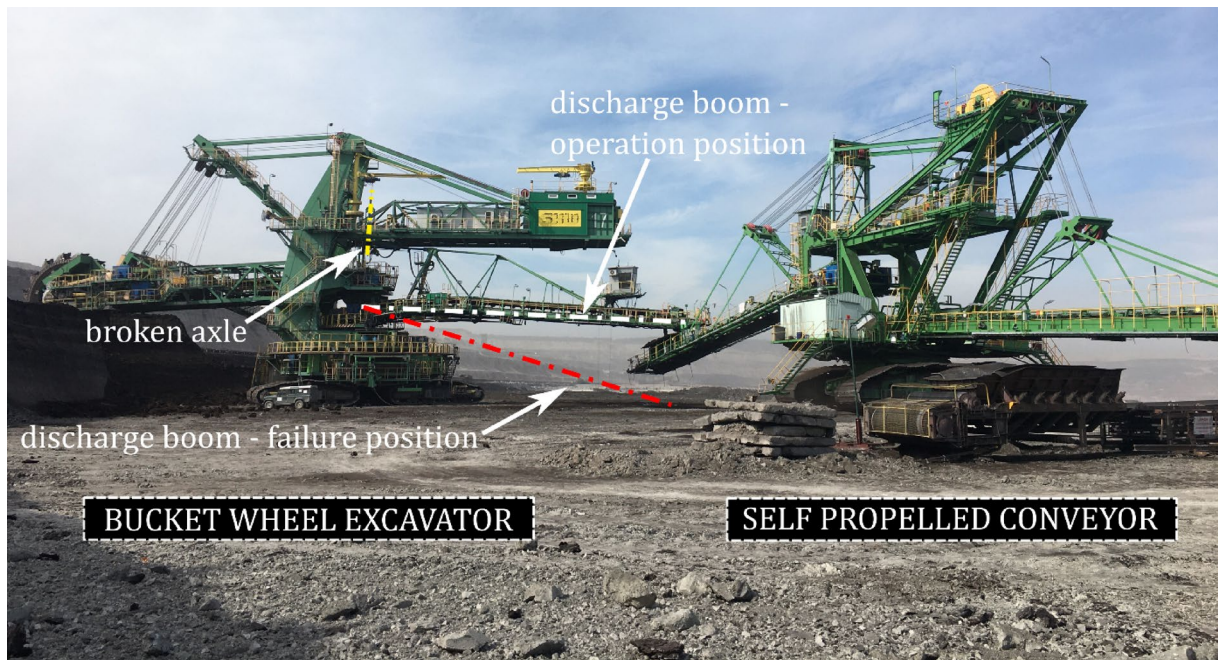


Fig. 3. General view of the excavator and conveyor before the failure.

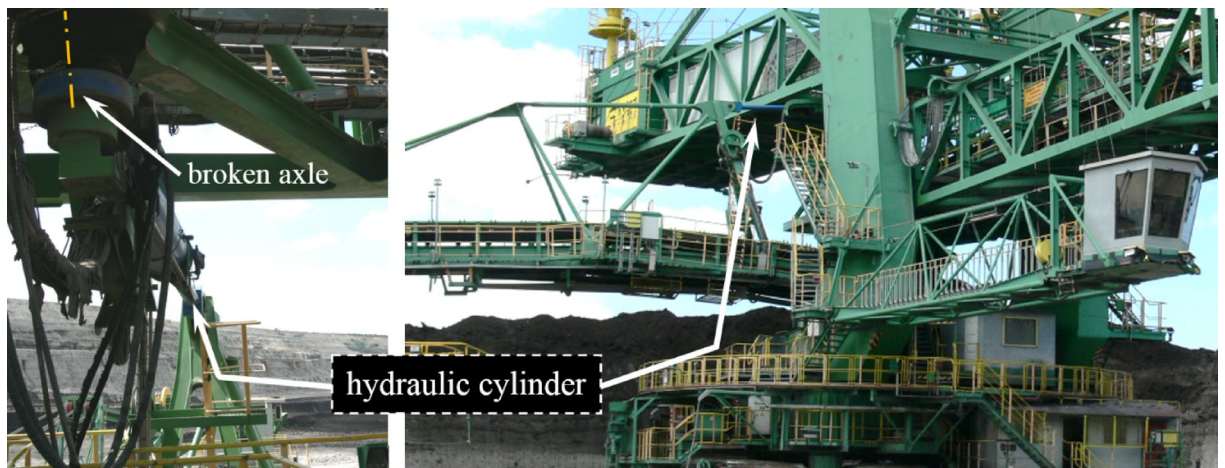


Fig. 4. Location of luffing hydraulic cylinder.

The axle failure shown in Fig. 5 caused an uncontrolled movement in the vertical direction of the entire discharge boom. The maximum height at which the end of the boom can be raised is 11.3 m. This means that there is a risk that the boom will fall from this height if the axle fails. Such a situation was a consequence of the failure discussed. As a result of axle breakage, the discharge boom fell on a self-propelled conveyor belt. This resulted in significant financial losses. The reasons for these losses were as follows. The first concerns material damage related to machine damage. The structure of the boom itself as well as the self-propelled belt conveyor was damaged. A view of the damaged structures after the failure is shown in Figs. 7 and 8. The second concern financial losses due to them being taken out of service for several months. According to data available in the literature<sup>24</sup>, one month of inability to use these machines brings losses of € 148 000 due to the lack of production.

The event shown in Figs. 7 and 9 had a huge impact on the operations of the owning company. It caused significant damage to the discharge boom of the bucket wheel excavator. For this reason, it had to be put out of service for many weeks to assess its technical condition and repair any damage found. An example of damage found during the technical assessment is shown in Figs. 9 and 10. Furthermore, the self-propelled conveyor belt was so badly damaged. It was necessary to rebuild a significant part of its carrying structure, especially the superstructure. This was associated with large financial losses and many months of difficult operation at the mine. Taking into account the above facts, it is important to find the cause of this failure. Especially since only 9 years have passed since the excavator was put into operation.

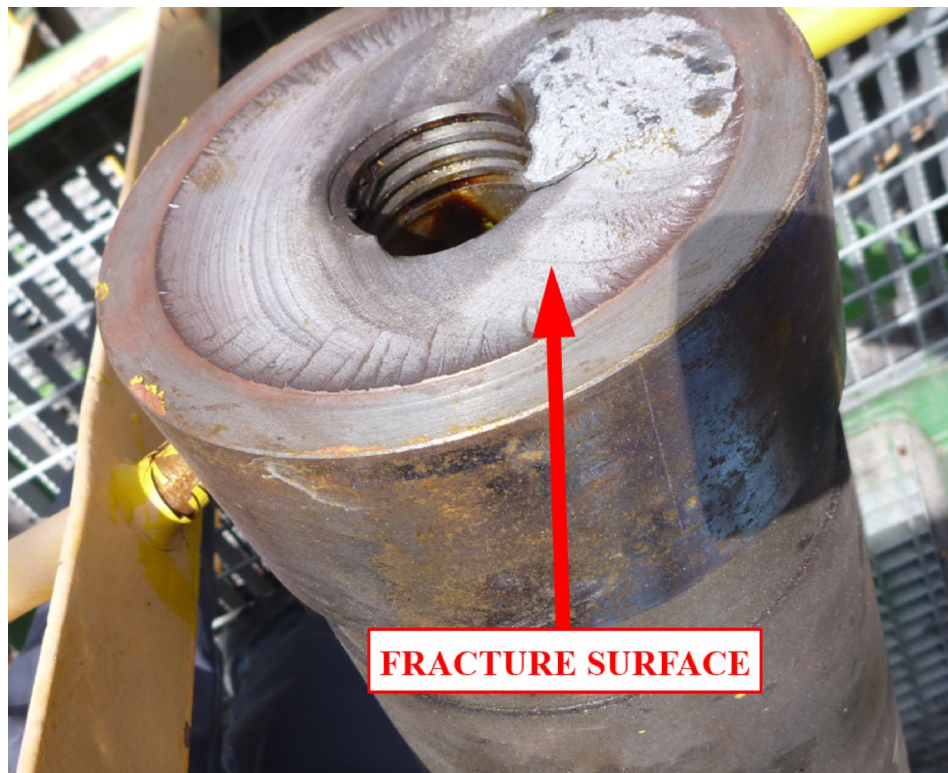


Fig. 5. Post failure view of fatigue fracture of a vertical axle of a damaged discharge boom.

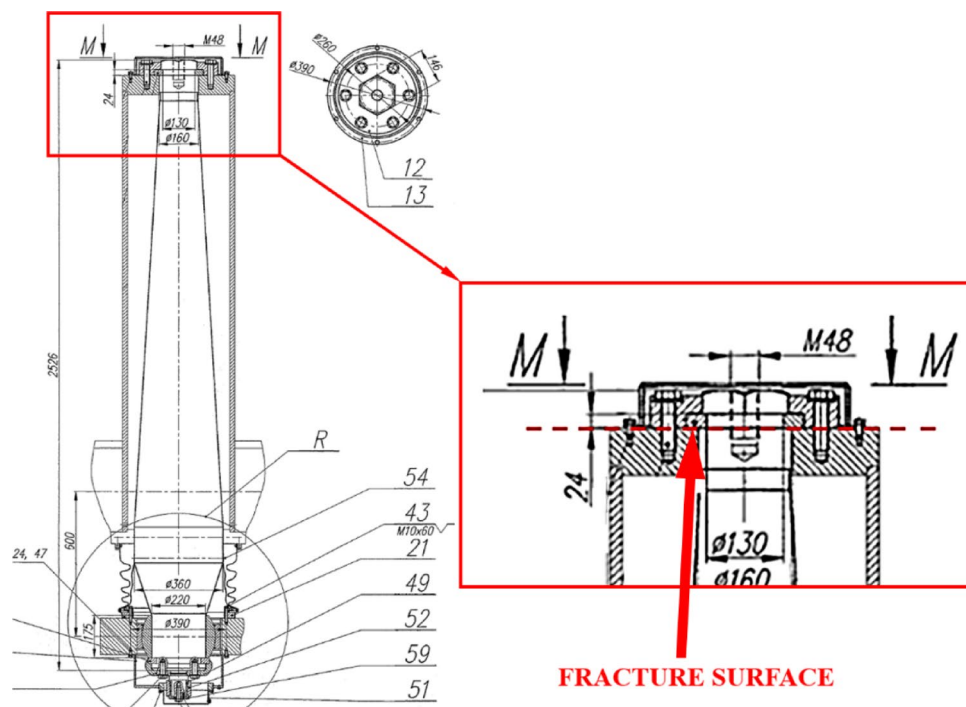


Fig. 6. Drawing showing whole damaged axle with cross section where axle was cut—marked with a red line (well visible on the magnified part of the drawing).



**Fig. 7.** View of the self-propelled conveyor after failure.



**Fig. 8.** Discharge boom of bucket wheel excavator (left side) and self-propelled conveyor (right side) after failure.



**Fig. 9.** Exemplary damage after a failure of the carrying structure of the discharge boom—plastic deformation.

### Fracture and material microstructure analysis

Analysis of the material microstructure aimed at verification of the material grade used to manufacture axle and finding reasons of the failure. These analyses have been realized with the use of broken axle pieces. Few test pieces were used for metallographic, microscopic, and strength studies<sup>25–29</sup>.

Firstly, macroscopic and fractography analysis was performed with use of stereoscope (SMT-800 type) and scanning electron microscope (Hitachi S-3400N). Fracture fractography was realized after impact resistance test for two different samples, taken both in longitudinal as well as in transverse direction to axle axis. In Fig. 11 brittle fracture is clearly visible in cases of both specimens. Further analysis proves that for broken axle, there is a fatigue fracture with slip bands and origin point next to the surface, what is well visible in Fig. 12. Final rupture zone has features of a ductile and brittle fracture. This zone is about 20% of the fracture, which indicates that the safety factor of axle was about 5. Such fracture mode was the result of a unidirectional bending. The initiation of



**Fig. 10.** Examples of damage after a failure of the carrying structure of discharge boom—cracks.

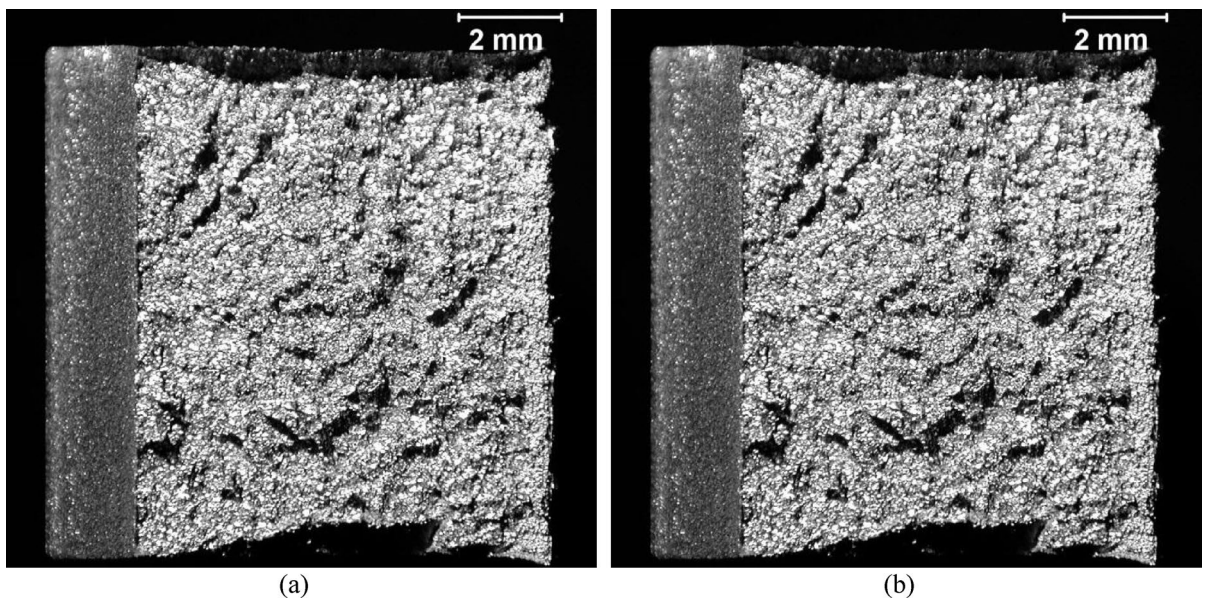


**Fig. 11.** Brittle fracture on the sample taken along longitudinal (a) and in transverse direction (b) to axle axis.

the fatigue fracture took place in the notch. It is shown in Fig. 13 as a cross section change with radius 0.84 mm, which is according to technical documentation of the axle<sup>25–29</sup>.

Next step was a microscopic research of samples in transverse axle cross sections. It was realized with the use of the metallographic microscope Olympus CK40M coupled with digital camera, in range of magnification from 50× to 1000×<sup>25,26</sup>. Before this, selected samples were a subject of micro-etching with use of Mi1Fe reagent. Received results showed clearly that microstructure is a nonhomogeneous ferritic-pearlitic structure, coarse-grained with bainite bands and a ferrite acicular structure having features of the Widmanstätten pattern (Fig. 14). Such a structure is a result of the cooling after hot processing. Strictly, such structure is not recommended for carrying structures elements subjected to high load due to the fact that Widmanstätten pattern is very sensitive to initiation and propagation of the fatigue fracture. It is obvious that such structure was responsible for huge decrease of the strength, mainly impact resistance of the axle and was reason of the fatigue crack initiation and growth. Definitely such material is not in accordance with material certificate, which clearly indicates that it should be material after hardening and tempering to hardness 235 ± 241 HB (highly tempered martensite). Brinell hardness tests conducted according to suitable standard showed that tested material has hardness much lower and equal to 211.38 ± 2.02 HB<sup>30</sup>.

Material properties were evaluated with use of tensile test according to suitable standard<sup>31</sup>. Test was conducted in temperature of 23 °C with use of testing machine VEB—model FPZ 100/1. In this case, three specimens have been tested. As a results, average values of the most important material properties have been evaluated and compared with material specification (Table 1). From Table 1 it is well visible that the material used to manufacture the broken axle differs greatly from the material according to the certificate.

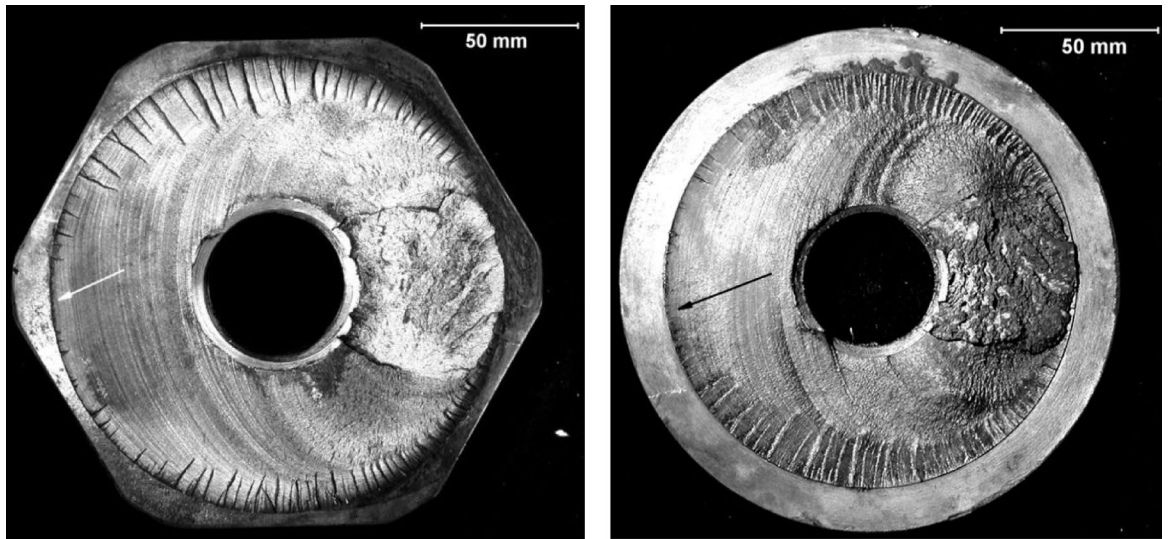


**Fig. 12.** Fatigue fracture with well visible slip lines in two different sections. The arrow indicates the fatigue origin point.

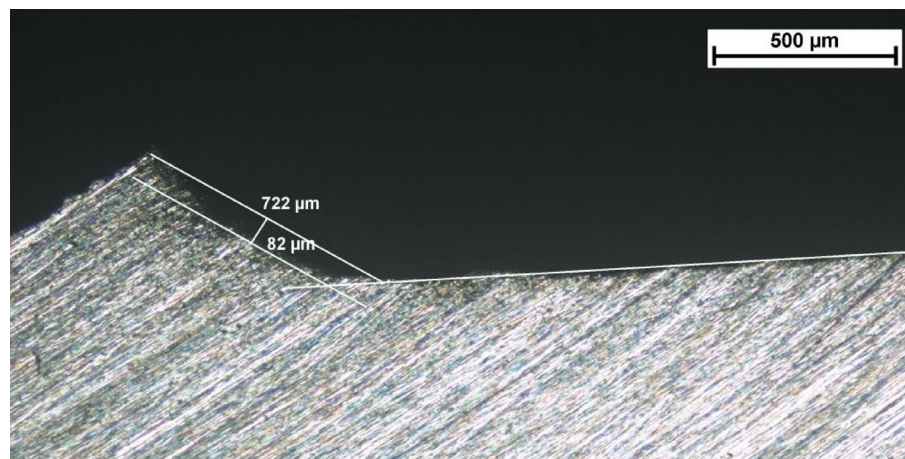


**Fig. 13.** Section parallel to shaft axis with area of cross section change, where the fatigue origin point was located. The lines show the chord and dimensions of the pit due to edge fillet with radius 0,84 mm.

Similar conclusions has been gathered after impact resistance investigation, that was realized with use of Charpy impact test<sup>32</sup>. Conducted test showed that impact work is equal to 11 J (kV150) or 13 J/cm<sup>2</sup> (kcV150) and 9 J (kV150) or 11 J/cm<sup>2</sup> (kcV150) in case of the longitudinal section and transverse section respectively. In the material certificate impact resistance is equal to 88.93 KCU2. In this case, according to the suitable standard PN-EN 10083-3 impact work (KV) should be at least 35 J, which is inconsistent with the real material used to manufacture the axle<sup>33</sup>.

### FEM analysis

The load analysis was carried out on the basis of the data provided by the machine designer. Due to the nature of the damage, combination for the H1b—fatigue load case was taken into account according to the DIN22261-2 standard. Permanent loads (deadweight E, incrustation V) and live loads (excavated material F, dynamic loads D) were assumed. Table 2 presents calculated loads in the luffing cylinder for three considered positions of the discharge boom. This load in the luffing cylinder is the force acting on the suspension axle as shown in Fig. 15. The maximum calculated force is  $F = 1499$  kN.

The next step was to create a geometrical model of the axis and its cooperating elements<sup>34</sup>. Solid finite elements were generated on the model in the upper support area (green color in Fig. 17), while in the rest of the model beam elements (blue color in Fig. 17) were considered. In addition, a constraint and a specified force were applied. In the most important part of the axle (area of breakage), the model was prepared with use of solid elements hexa 8 (in outer regions of axle) and tetra 10 (inner axle region). The rest part of the shaft has

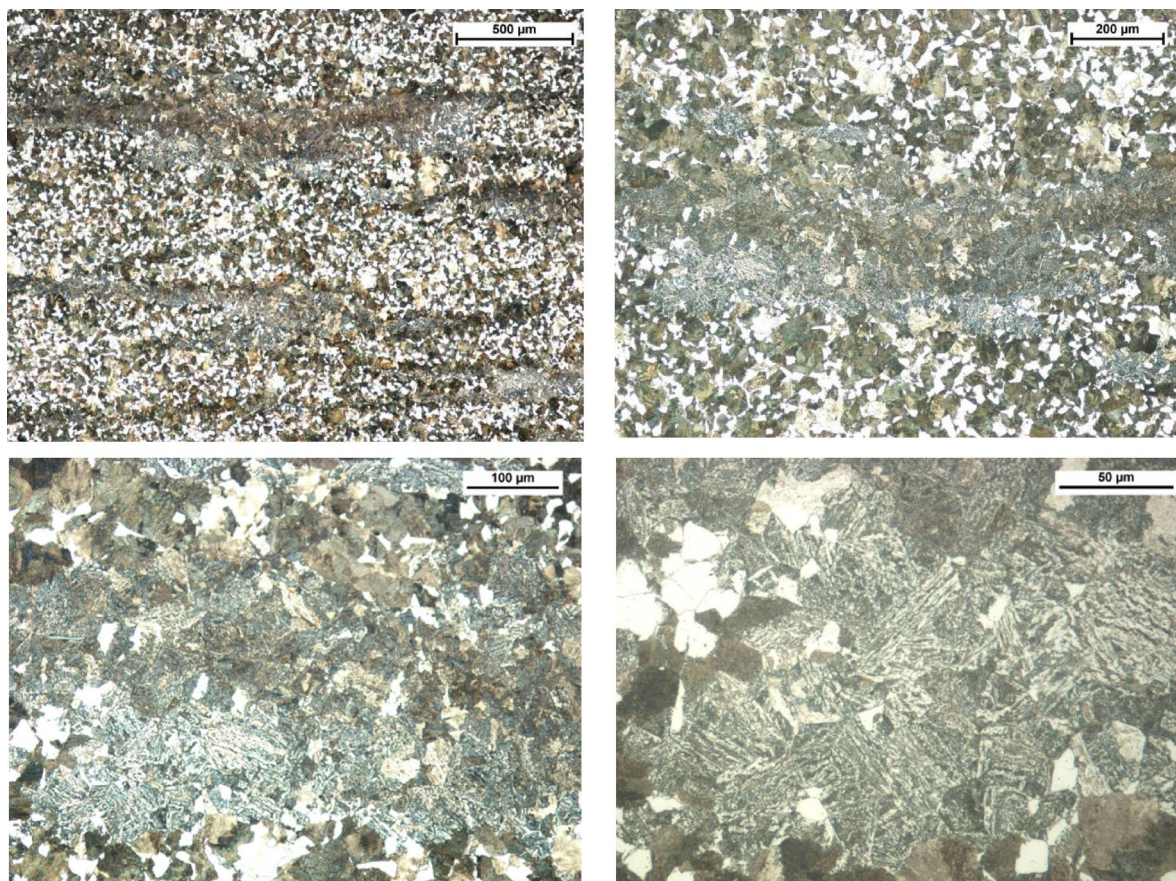


**Fig. 14.** Nonhomogeneous ferritic-pearlitic structure, coarse-grained with bainite bands and a ferrite acicular structure having features of the Widmanstätten pattern seen in four different magnification.

Material property	Tested samples	According to material certificate	According to PN-EN 10,083–3 <sup>33</sup> (Ø 160–250 mm)
Yield strength $R_{p0.2}$	433 MPa	643 MPa	min. 500 MPa
Tensile strength $R_m$	749 MPa	828 MPa	750–900 MPa
Elongation at fracture $A_5$	23%	19.6%	> 14%

**Table 1.** Mechanical properties of the material received after tensile tests and taken from the material certificate.

Load case	Discharge boom luffing position	Luffing cylinder force components (Fig. 14) [kN]		Total luffing cylinder force F [kN]
		$F_x$	$F_z$	
H1b	up	1451	– 11	1451
	horizontal	1464	219	1481
	low	1444	402	1499

**Table 2.** Loads in the luffing cylinder for three considered positions of the discharge boom (H1b load case according to DIN22261-2 standard).

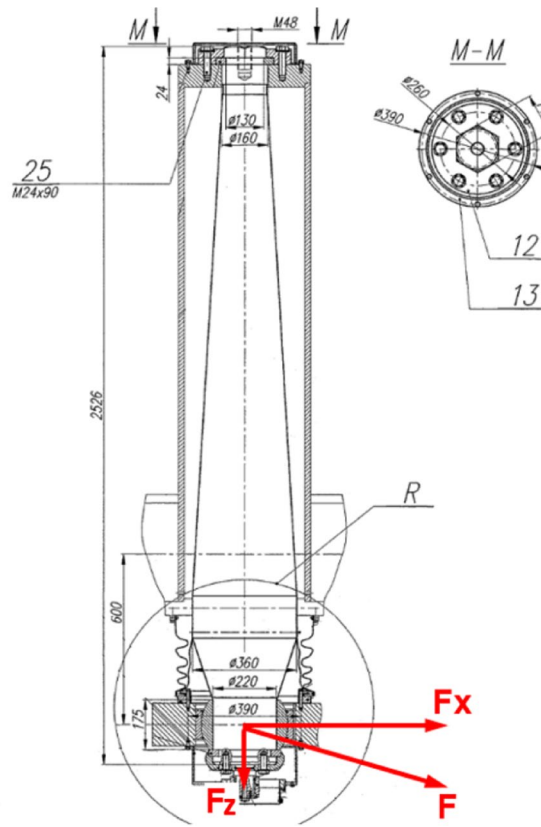


**Fig. 15.** Diagram of load operation on the discharge boom suspension axle.

been modeled with use of beam elements. The connection between beam and solid elements of the axle was realized with use of special element Rigid Bar Element. The total number of elements in the model was almost 130 000 and the total number of nodes was over 146 000. The software used to run analysis of the basic axle model was NX I-deas(R) software ver. 6.1 and Siemens NX software ver. 2206 (<https://plm.sw.siemens.com>). In the complete calculation model, the contact connections in the upper axle bearing and the individual securing elements were also defined. The joint between the axle and fastener has been prepared with defined neighboring surfaces contact. These steps are shown in Figs. 16, 17 and 18.

Highly stressed areas were identified during the calculations for two variants of material characteristics:

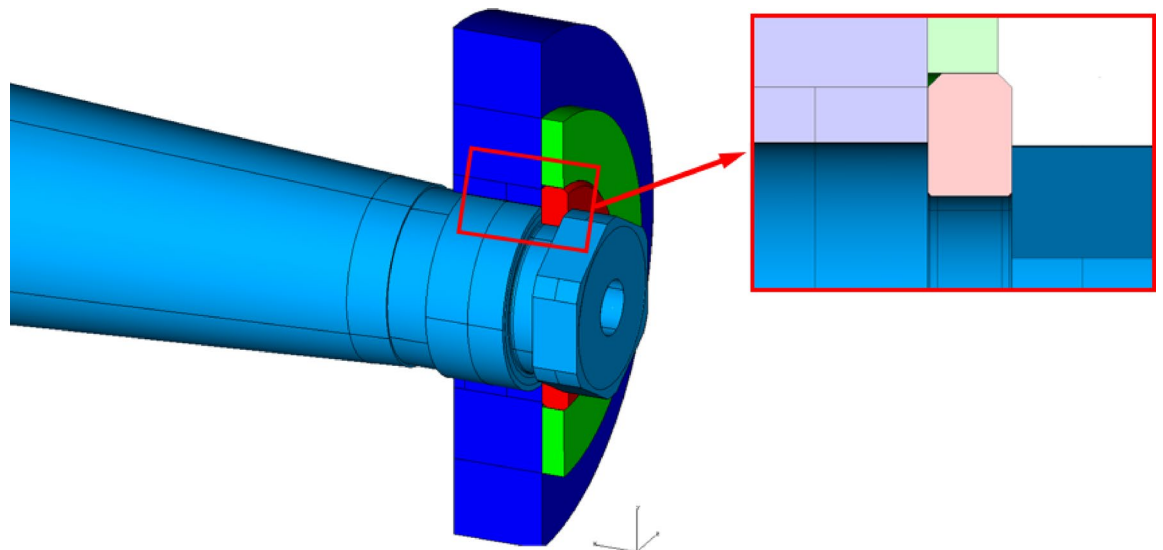


**Fig. 16.** Details of the the geometrical model of axle and the securing elements (cross-section and detailed view).

- Linear elastic material (Fig. 19)  $\sigma_{\text{HMHmax}} = 1280 \text{ MPa}$
- Non-linear, elastic–plastic material (Fig. 20)  $\sigma_{\text{HMHmax}} = 471 \text{ MPa}$

The axle fracture did not occur at the point of highest stress level, but on the other side of the circlip groove. During the geometrical verification of the securing ring, it was found to be deformed due to the way the joint was constructed. As a result, the circlip partially took over the function of the radial bearing and caused an additional bending force at the axle end, generating stress concentration at the fracture site. A diagram of this phenomenon is shown in Fig. 21. Contact marks on both diameters are clearly visible on the protective ring, axle, and protective cover and are shown in Fig. 22.

For these types of working conditions, additional numerical simulations were carried out with consideration of non-linear, elastic–plastic material, and the stress effort of the critical region was identified. A variant was used where the discharge boom is in the low position, which corresponds to the maximum value of the total luffing cylinder force  $F$  (Table 2). The maximum stresses level in the fracture region increased by about 40% compared to the initial state (without ring deformation Fig. 20) and amounted to 649 MPa (Fig. 23). Under such operating conditions, at the point of axle breakage, there was a stress level in the low-cycle range, since the value of stresses in a cycle is in excess of the yield strength of a material (described in Table 1). It resulted in limited fatigue strength, which consequently contributed to the occurrence of failure.

### Experimental verification of calculations

After repair, studies have been carried out to check the actual loads acting on the discharge boom axle. A measurement system with strain gauges located on the eye of the luffing hydraulic cylinder (Fig. 24) and data recorder was build. In the next step, the system was calibrated and the load on the suspension system was recorded in variable excavator operating conditions. This load recorded during the travel of the excavator, with the discharge boom perpendicular to the direction of travel, is shown in Fig. 25. Table 3 shows the maximum values of the load changes recorded during the tests.

The operating loads acting on the axle, identified during tests consist of the self-weight of the boom including material incrustation (static component) and life loads presented in Table 3 (dynamic component). The static loads resulting from self-weight were verified by checking hydraulic luffing cylinder loads and no significant differences were observed in comparison to design data. The total operating loads acting on the axle were compared with the theoretical values calculated with consideration of the DIN22261-2 standard, presented in Table 2. The maximum theoretical load in the luffing cylinder equals:

$$F_{\text{th}} = 1499 \text{ kN}$$

The maximum measured load in the luffing cylinder equals:

$$F_{\text{exp}} = 1769 \text{ kN}$$

Identified total operating load acting on the axle is 18% higher than calculated according to the DIN22261-2 standard. During the measurements, an increase in loads was observed in the lower position of the boom, especially during machine traveling. The measurements were carried out for the full spectrum of technological loads of the excavator and the maximum values, resulting from all operational loads, were taken into account in the calculations.

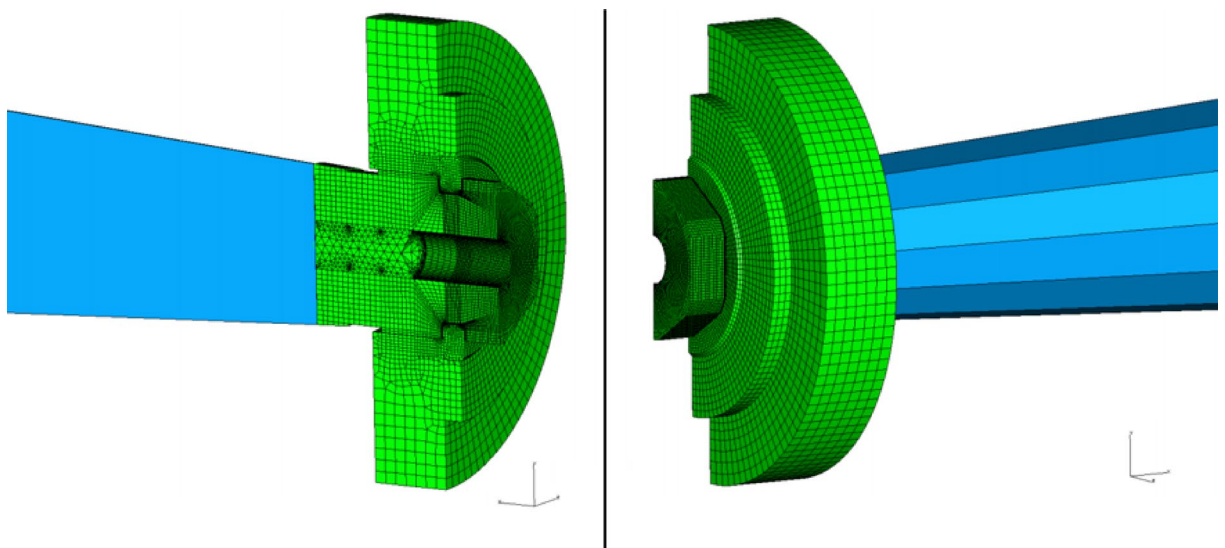


**Fig. 17.** Details of the FEM model of axle and securing elements (cross-section view).

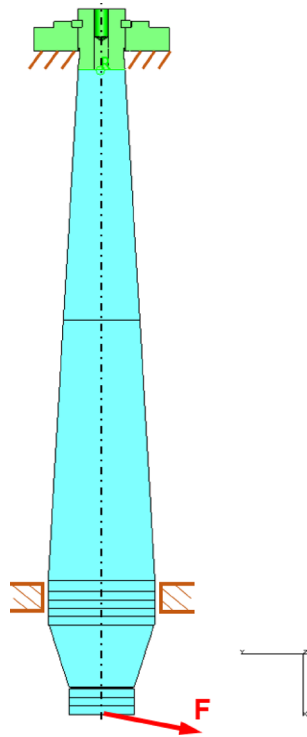


**Fig. 18.** Computational model with applied boundary conditions.

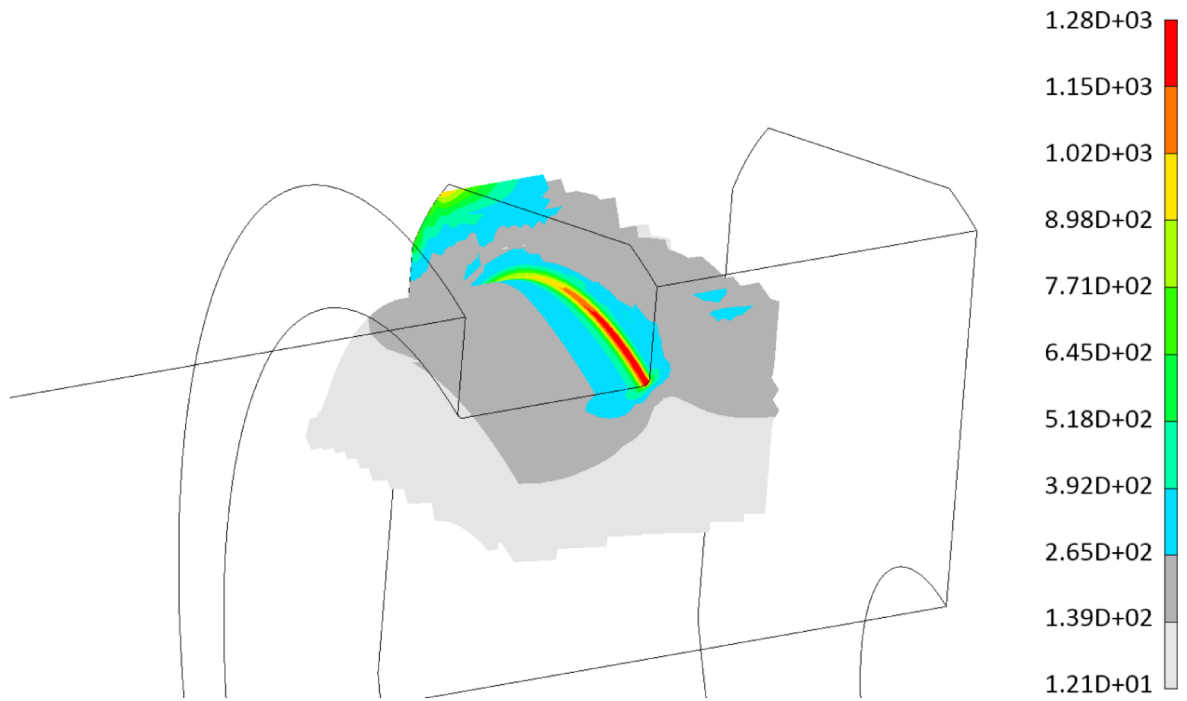


**Fig. 19.** Equivalent Von Mises stress distribution in MPa—linear elastic material.

### Modification of the discharge boom suspension

In order to bring the machine back into operation it was necessary to modify the original suspension of the discharge boom where the broken axle is used. Modification was based on the change of its design and ensuring appropriate material quality. The final design of the axle is presented in Fig. 26 (upper support) and in Fig. 27a (overall view). Compared to Fig. 6 it is well visible that the sensitivity to fatigue crack in the notch was decreased

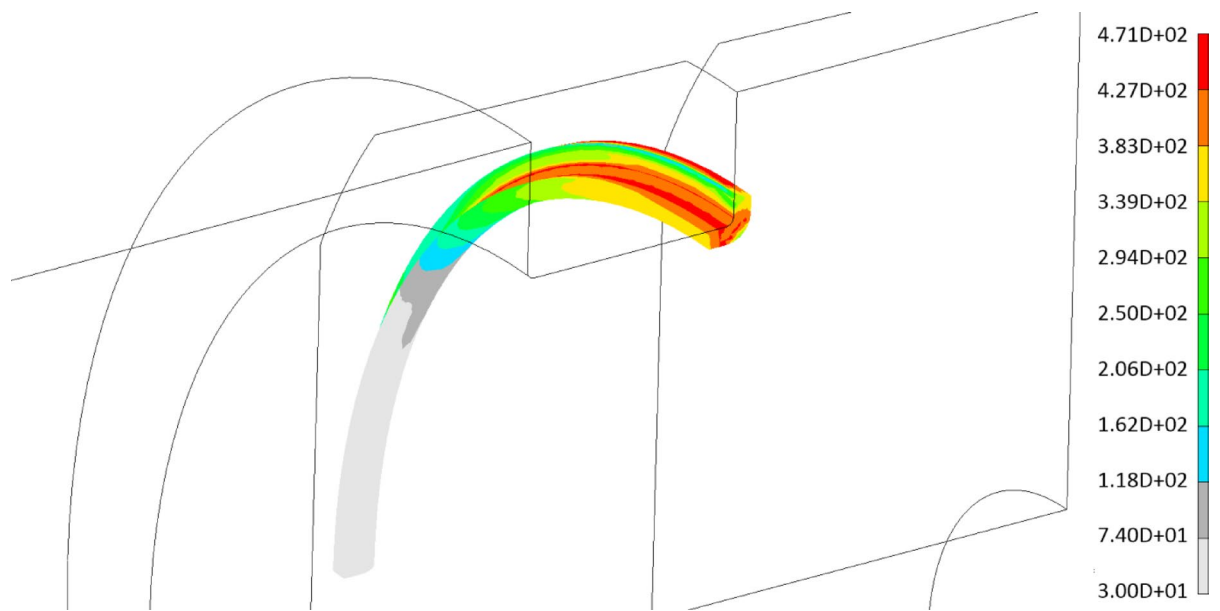


**Fig. 20.** Equivalent Von Mises stress distribution in MPa—non-linear, elastic–plastic material.

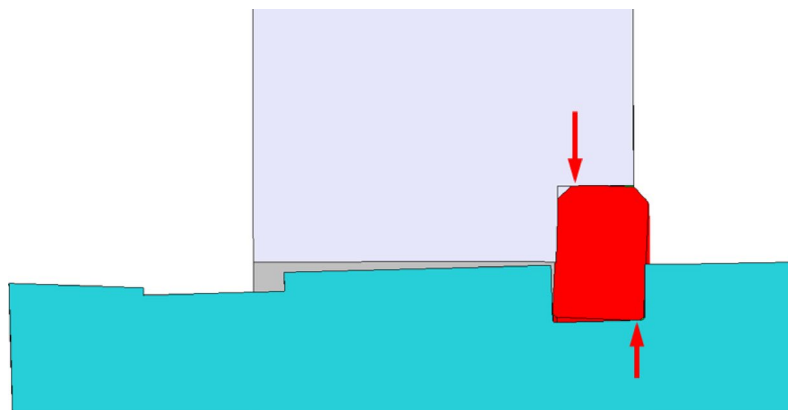


**Fig. 21.** Diagram of the acting forces on the axle and the seat of the deformed circlip.

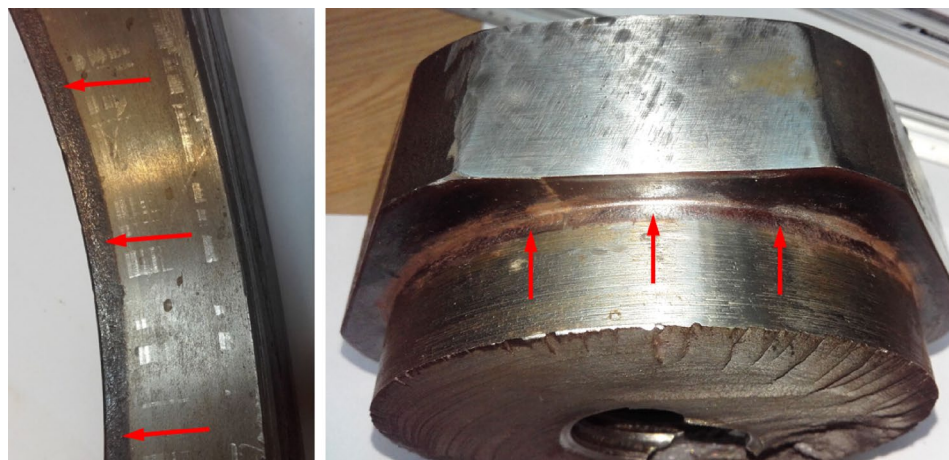


**Fig. 22.** Contact marks on the protective ring and axle circlip groove.

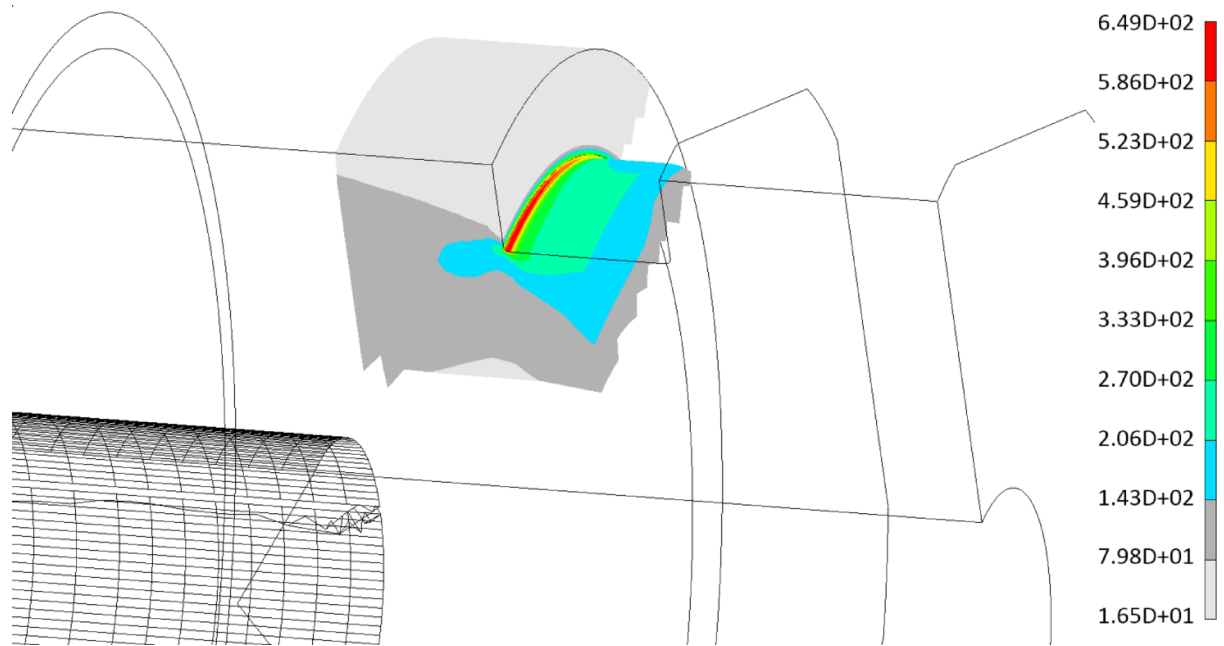


**Fig. 23.** Equivalent Von Mises stress distribution in MPa—real boundary conditions.



**Fig. 24.** Location of strain gauges.

due to replacement of the groove with two spherical bearings (GE-200AW and GE-180-AW Fig. 26) and an additional axle in the most vulnerable joint. The new suspension axle was manufactured from steel 40HM with a suitable microstructure without the Widmanstätten pattern to fulfill PN-EN 10083-3 standard<sup>33</sup> requirements.

The new design of the axle and its upper support has been verified with use of FEM<sup>34</sup>. Firstly, a solid geometrical model of the axle and neighboring elements has been created (Fig. 27a). The neighboring elements considered in the simulation of both the original and modified axles are the upper and lower bearing hubs, the upper axle vertical support elements. In the upper part of the axle, contact connections were defined between these elements in order to correctly consider the load transmission. On this basis, model has been meshed with use of solid elements (Fig. 27b). Finally, a simulation model with boundary condition applied according to the scheme shown in Fig. 27 c has been created and then calculated. The force applied as a load acting onto axle was equal to  $F = 1769\text{kN}$ , which is maximal value received from tests on the real object described in previous section.

As a result equivalent Von Mises stress distribution has been received, which is shown in Fig. 28. From these calculations it is well visible, that maximal stresses are in the new axle in its lower part and the value of this stresses is much below yield point of the material, which is 643 MPa in case of steel 40HM. These results differ significantly compared to broken axle design, since maximal stresses are much lower and are not located in the notch placed in the upper support nut, close to lower axle support.

The fatigue strength of the new axle was calculated with the assumption, that maximal load identified during tests on real object is representative of fatigue load. Under such conditions, the allowable fatigue stress is equal to

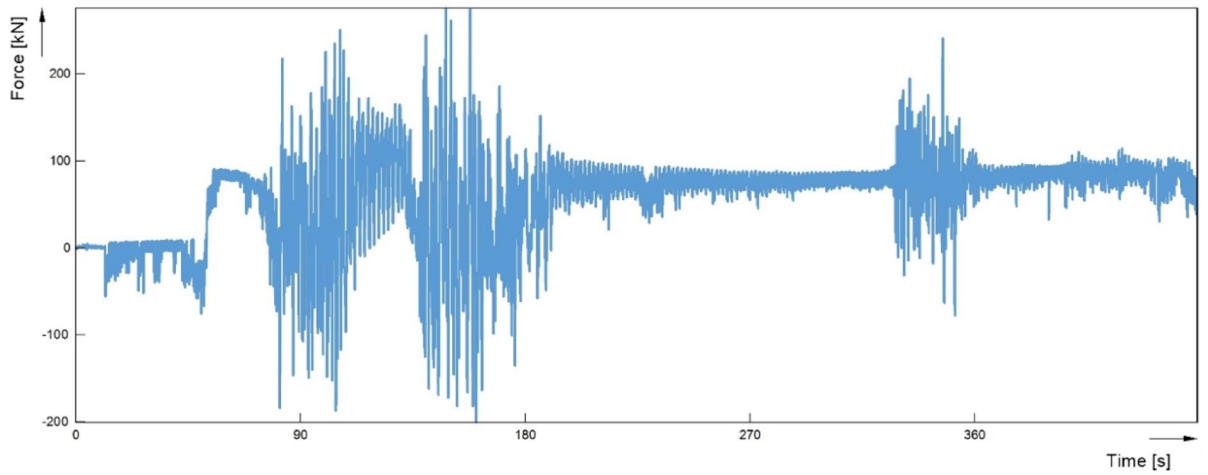


Fig. 25. Course of recorded variable loads.

Load case	$\Delta$ max [kN]
Traveling. Bucket wheel boom parallel to the direction of travel	283.6
Traveling. Bucket wheel boom perpendicular to the direction of travel	465.6
Excavating	374.6
Activation of the rotation drive and rotation of the bucket wheel boom after a longer standstill	157.4

Table 3. Maximum values of the range of load changes recorded during tests.

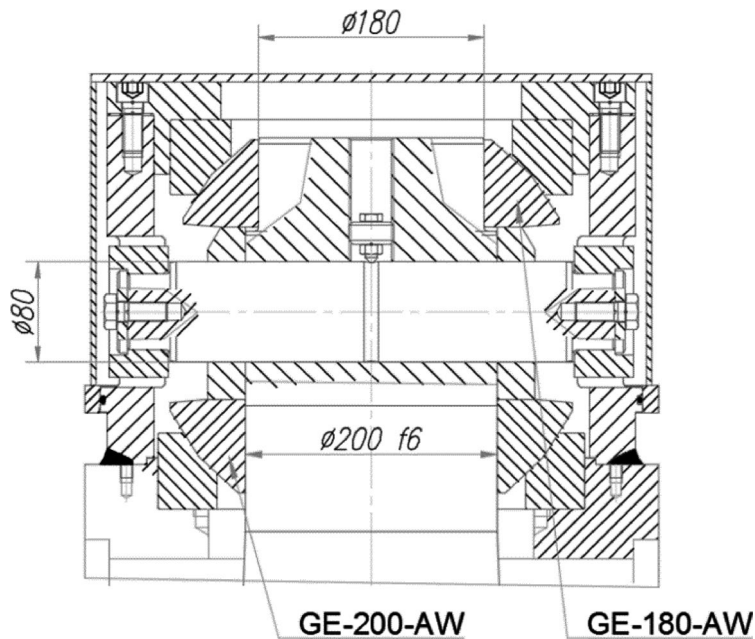
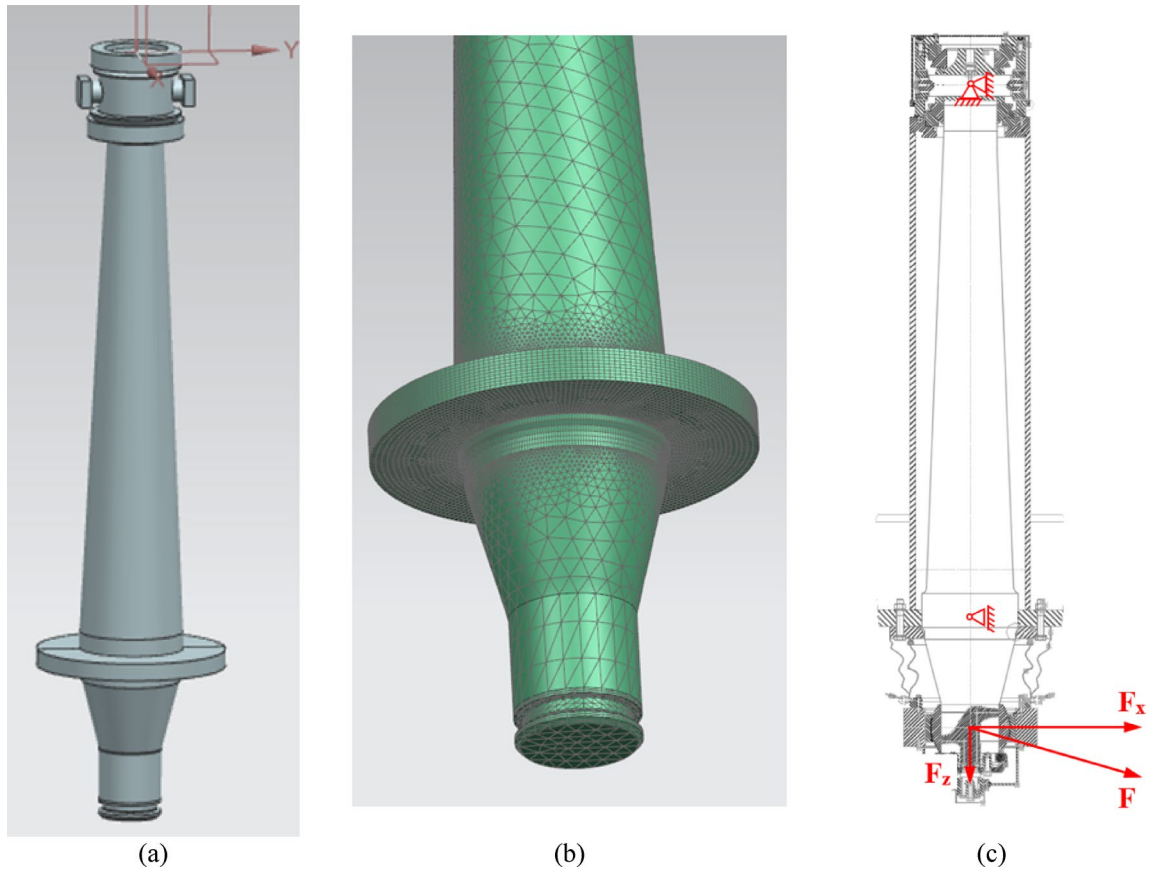


Fig. 26. New design of the vertical axle upper support.

$k_g = 0.45R_m^{35}$ . In case of axle made of steel 40HM and with consideration of material tests it was conservatively assumed that  $k_g$  is equal to 337 MPa. Comparing maximal Von Mises stresses received thanks to FE analysis it can be concluded that:

$$s_{max} = 212 \text{ MPa} < k_g = 749 * 0.45 = 337 \text{ MPa}$$

It means that the allowable fatigue stress limit is not exceeded in the case of a new axle.



**Fig. 27.** Geometrical (a) and discrete (b) model of the new design of the discharge boom suspension with scheme of the applied boundary conditions to the axle (c).

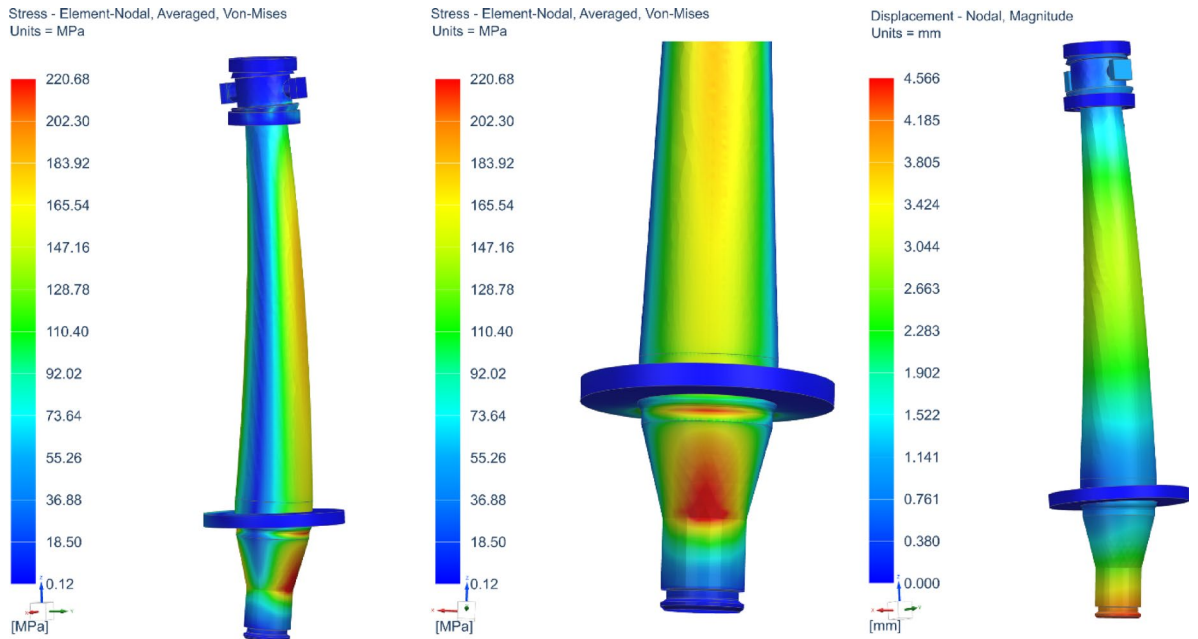


**Fig. 28.** Equivalent Von Mises stress distribution along the structure of newly designed axle (overall view – left, area with maximal stresses—center) and displacement (on the right).

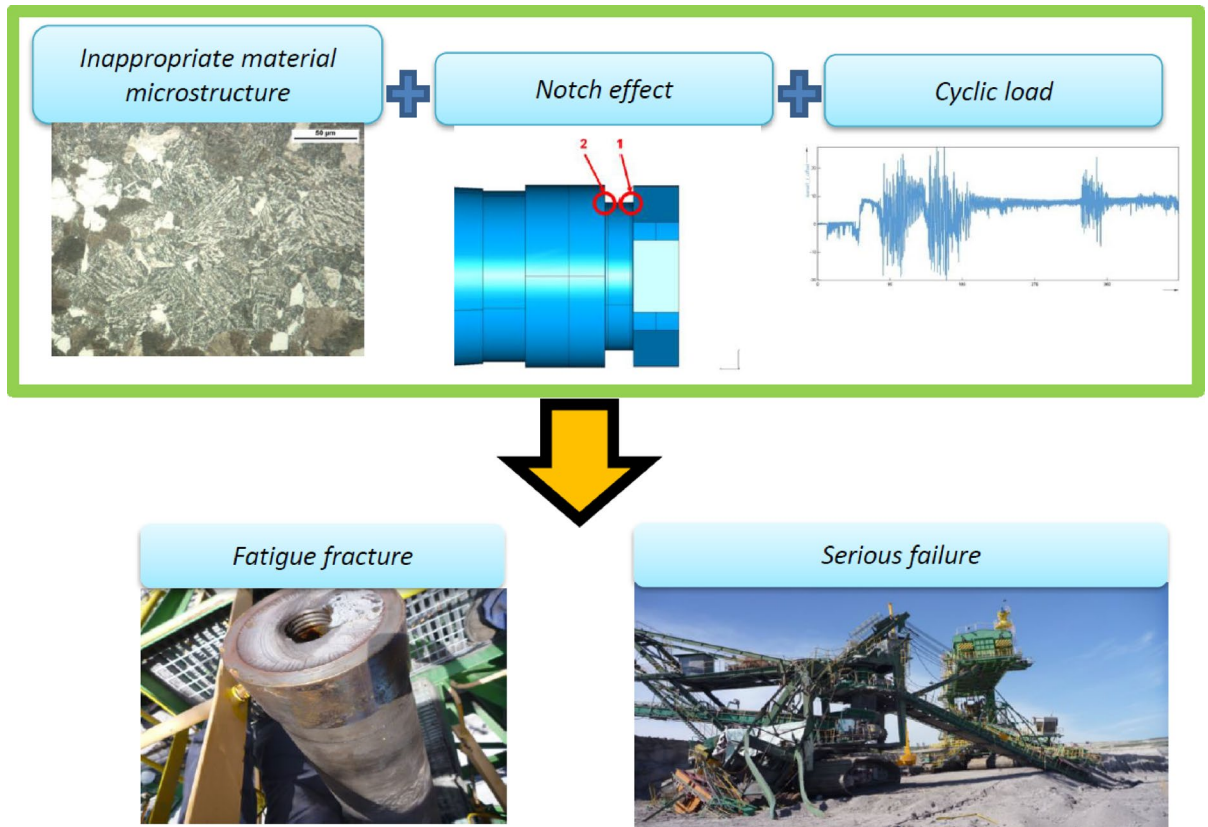


**Fig. 29.** Scheme showing reasons of the serious failure.

## Discussion

Presented article was focused on failure analysis of the discharge boom suspension of the bucket wheel excavator. Unexpected axle damage occurred during regular operation of the machine. As a result of the failure of this element, the discharge boom fell to the self-propelled conveyor boom causing catastrophic failure. Extensive root cause analysis was carried out. The causes of the failure have been found due to the fracture and material analysis. Fracture of the broken cross section proved that it was mainly due to fatigue, which was supported by well-visible slip bands. The rapture zone of fracture was measured and compared with fatigue fracture zone to calculate the static safety factor. The static fracture zone was 20% of the section, which gives the static safety factor was about 5. The fatigue fracture initiation point was located in the notch of the axle (change of cross section in the groove visible in Fig. 6).

Material microstructure verification showed that there was an undesirable ferrite acicular structure with features of the Widmanstätten pattern. Such a structure is not suitable for carrying structural elements subjected to high loads, especially varying loads, because of its sensitivity to the initiation and propagation of fatigue crack. Investigation of the mechanical properties of the axle material proved that it was not compatible with the attached material certificate and should not be used in the case of such a demanding object.

A further step was focused on the axle strength analysis. It was made with the use of FEM and was aimed at evaluation of the stress level in the notch, where axle was broken under normative loads<sup>36</sup>. Obtained results proved that the maximal values of von Mises stresses were located exactly at the notch of the axle. This value was equal to 649 MPa in the case of elastic plastic material considered. Such stress concentration of the stresses that are changing during excavator operation, in conjunction with the notch effect and insufficient material microstructure, caused failure of the axle and as a consequence, fall of the excavator discharge boom. The plastic zone in the notch area is very small and the fatigue process in this zone occurred within the range of low-cycle fatigue strength. This caused the initiation of a fatigue crack, its development and complete fracture. The relatively high (5) static safety factor of the axle indicates its globally correct dimensions, but the structural notch and the resulting plastic deformations caused the initiation of the fatigue process and its development. It need to be underlined that strength calculations were performed for nominal loads that varies from real values what was proved by additional measurements on the real object after repair (18% greater force).

Ultimately, it can be stated that the described serious failure was caused by fatigue fracture. It was due to the combination of three important factors, which is schematically shown in Fig. 29. These factors were inappropriate material microstructure, notch effect, and cyclic load.

The repair of the excavator was based on the change of its design and material. The final design of the axle is presented in Fig. 26. Compared to Fig. 6 it is well visible that sensitivity to fatigue crack in the notch was decreased thanks to replacement of the groove with two spherical bearings and additional axle in the most

vulnerable joint. The new suspension axle was manufactured from material with a suitable microstructure without the Widmanstätten pattern. Also, the design of the axle was changed.

## Conclusions

The conclusions related to failure of the discharge boom suspension of bucket wheel excavator are presented below.

1. Fracture of the broken cross section showed the fatigue phenomena by well-visible slip bands.
2. The static safety factor was calculated as 5 based on the rupture zone fracture cross section.
3. The fatigue fracture initiation point was located in the notch of the axle (in Fig. 6).
4. Material microstructure verification showed an undesirable ferrite acicular structure with features of the Widmanstätten pattern observed in the axle material, not suitable for carrying structural elements subjected to high loads
5. Based on FEA calculations the maximal values of von Mises stresses were located exactly at the fracture areas of the axle.
6. Such stress concentration of the variable stresses, in conjunction with the notch effect and material microstructure, caused failure of the axle.
7. The nominal design loads are lower for 18% than the one measured on the machine after repair. This is additional factor that contributed the failure of the axle.

## Data availability

The datasets used and/or analysed during the current study available from the corresponding author on reasonable request.

Received: 19 May 2025; Accepted: 23 July 2025

Published online: 04 August 2025

## References

1. Honus, S., Bocko, P., Bouda, T., Ristović, I. & Vulić, M. The effect of the number of conveyor belt carrying idlers on the failure of an impact place: A failure analysis. *Eng. Fail. Anal.* **77**, 93–101. <https://doi.org/10.1016/j.engfailanal.2017.02.018> (2017).
2. Đorđević, B., Sedmak, S., Tanasković, D., Gajin, M. & Vučetić, F. Failure analysis and numerical simulation of slab carrying clamps. *Frattura Integrità Strutturale* **15**(55), 336–344. <https://doi.org/10.3221/IGF-ESIS.55.26> (2020).
3. Alpsten G. Causes of structural failures with steel structures. In *IABSE Symposium Report 2017*; 107(01): 1–9. International Association for Bridge and Structural Engineering.
4. Krejsa, M. Probabilistic failure analysis of steel structures exposed to fatigue. *Key Eng. Mater.* **577**, 101–104. <https://doi.org/10.4028/www.scientific.net/KEM.577-578.101> (2014).
5. Van Do, V. N. The behavior of ductile damage model on steel structure failure. *Procedia Eng.* **142**, 26–33. <https://doi.org/10.1016/j.proeng.2016.02.009> (2016).
6. Yamano, Y., Tsuji, K., Mizoe, H., Muroi, T. & Yamakawa, Y. Nonlinear repairing analysis of damaged transmission tower under different seasonal loads and support movement: Assessment of repair measures and strength recovery. *Eng. Struct.* **333**, 120029. <https://doi.org/10.1016/j.engstruct.2025.120029> (2025).
7. Przybyłek, G. & Więckowski, J. Method of assessing the technical condition and failure of overhead cranes designed to work in difficult conditions. *Case Stud. Constr. Mater.* **16**, e00811. <https://doi.org/10.1016/j.cscm.2021.e00811> (2022).
8. Yıldırım, H. C., Leitner, M., Marquis, G. B., Stoschka, M. & Barsoum, Z. Application studies for fatigue strength improvement of welded structures by high-frequency mechanical impact (HFMI) treatment. *Eng. Struct.* **106**, 422–435. <https://doi.org/10.1016/j.engstruct.2015.10.044> (2016).
9. Misiewicz, R. & Więckowski, J. S. The assessment of the technical condition of complex fatigued load-carrying structures. *Appl. Sci.* **11**(6), 2449. <https://doi.org/10.3390/app11062449> (2021).
10. Brkić, A., Maneski, T., Ignjatović, D., Jovančić, P. D. & Brkić, V. S. Diagnostics of bucket wheel excavator discharge boom dynamic performance and its reconstruction. *Eksploracija i Niezawodność* **16**(2), 188–197 (2014).
11. Bošnjak, S. M., Arsić, M. A., Zrnić, N. Đ., Rakin, M. P. & Pantelić, P. Bucket wheel excavator: Integrity assessment of the bucket wheel boom tie-rod welded joint. *Eng. Fail. Anal.* **18**(1), 212–222. <https://doi.org/10.1016/j.engfailanal.2010.09.001> (2011).
12. Danicic, D. & Maneski, T. The structure failure of the discharge boom of bucket wheel excavator C 700 S due to dynamic effects. *Struct. Integr. Life Integritet i Vek Konstruktivna* **12**(1), 43–46 (2012).
13. Rusiński, E., Czmochoński, J., Iluk, A. & Kowalczyk, M. An analysis of the causes of a BWE counterweight boom support fracture. *Eng. Fail. Anal.* **17**(1), 179–191. <https://doi.org/10.1016/j.engfailanal.2009.06.001> (2010).
14. Araujo, L. S. et al. Failure of a bucket-wheel stacker reclaimer: Metallographic and structural analyses. *J. Fail. Anal. Preven* **12**, 402–407. <https://doi.org/10.1007/s11668-012-9575-z> (2012).
15. Andruszko, J., Moczko, P., Pietrusiak, D., Przybyłek, G. & Rusiński, E. Analysis of the causes of fatigue cracks in the carrying structure of the bucket wheel in the SchRs4600 excavator using experimental-numerical techniques. In *Proceedings of the 14th International Scientific Conference: Computer Aided Engineering, 2018; CAE 2018. Lecture Notes in Mechanical Engineering* (eds Rusiński, E. & Pietrusiak, D.) (Springer, Cham, 2019). [https://doi.org/10.1007/978-3-030-04975-1\\_3](https://doi.org/10.1007/978-3-030-04975-1_3).
16. Djurdjevic, D., Maneski, T., Milosevic-Mitic, V., Andjelic, N. & Ignjatovic, D. Failure investigation and reparation of a crack on the boom of the bucket wheel excavator ERS 1250 Gacko. *Eng. Fail. Anal.* **92**, 301–316. <https://doi.org/10.1016/j.engfailanal.2018.05.015> (2018).
17. Moczko, P., Pietrusiak, D. & Więckowski, J. Investigation of the failure of the bucket wheel excavator bridge conveyor. *Eng. Fail. Anal.* **106**, 104180. <https://doi.org/10.1016/j.engfailanal.2019.104180> (2019).
18. Gnjatović, N. B., Bošnjak, S. M., Milenović, I. L. & Stefanović, A. Z. Bucket wheel excavators: Dynamic response as a criterion for validation of the total number of buckets. *Eng. Struct.* **225**, 111313. <https://doi.org/10.1016/j.engstruct.2020.111313> (2020).
19. Rusiński, E., Czmochoński, J., Moczko, P. & Pietrusiak, D. Challenges and strategies of long-life operation and maintenance of technical objects. *FME Trans.* **44**, 219–228 (2016).
20. Moczko, P., Olejnik, M. J. & Więckowski, J. S. Thermo-chemical degradation of industrial installations-experimental and numerical technical condition assessment. *Case Stud. Constr. Mater.* **17**, e01685. <https://doi.org/10.1016/j.cscm.2022.e01685> (2022).
21. Moczko, P., Pietrusiak, D. & Rusiński, E. Material Handling and Mining Equipment - International Standards Recommendations for Design and Testing. *FME Transactions* **46**, 291–298 (2018).

22. Grabowski, P., Jankowiak, A. & Marowski, W. Fatigue lifetime correction of structural joints of opencast mining machinery. *Eksploatacja I Niezawodnosc Maint. Reliab.* **23**(3), 530–539. <https://doi.org/10.17531/ein.2021.3.14> (2021).
23. Babiarczyk, S. & Dudek, D. Kronika awarii i katastrof maszyn podstawowych w polskim górnictwie odkrywkowym. Oficyna Wydawnicza Politechniki Wrocławskiej (2007). In Polish.
24. Bugarić, U., Tanasijević, M., Polo Vina, D., Ignjatović, D. & Jovanić, P. Lost production costs of the overburden excavation system caused by rubber belt failure. *Eksploatacja i Niezawodność Maint. Reliab.* **14**(4), 333–341 (2012).
25. Mechanics and Mechanisms of Fracture—An Introduction, Liu, Alan F., ASM International 2005
26. Macek, W., Robak, G., Żak, K. & Branco, R. Fracture surface topography investigation and fatigue life assessment of notched austenitic steel specimens. *Eng. Fail. Anal.* <https://doi.org/10.1016/j.engfailanal.2022.106121> (2022).
27. Mueller, W. M. & McCall, J. L. *Metallographic Specimen Preparation: Optical and Electron Microscopy* (Springer, New York, 2012).
28. Brooks, C. R. & McGill, B. L. The application of scanning electron microscopy to fractography. *Mater. Charact.* **33**(3), 195–243 (1994).
29. Strnadel, B. New Methods of Damage and Failure Analysis of Structural Parts, Selected, peer reviewed papers from the conference "New Methods of Damage and Failure Analysis of Structural Parts", September 10-14, 2018, Technical University of Ostrava-VSB, Czech 2019.
30. Standard PN-EN ISO 6506-1:2008P: Metallic materials—Brinell hardness test.
31. Standard PN-EN ISO 6892-1:2010: Metallic materials—Tensile testing
32. Standard PN-EN-ISO 148-1:2010E: Charpy pendulum impact test
33. Standard PN-EN 10083-3: Steels for quenching and tempering—Part 3: Technical delivery conditions for alloy steel
34. Zienkiewicz O. C. & Taylor R. L. *The Finite Element Method*. Vol. 1, Vol. 2 (McGrawHill Book Company, London 1991).
35. Kocańda, S. & Szala, J. Basics of fatigue calculations, (*in Polish*). Państwowe Wydawnictwa Naukowe, Warszawa (1985).
36. Standard PN-G-47000-2: Excavators, spreaders and auxiliary equipment in opencast lignite mines - Part 2: Calculation principles (based on standard DIN 22261-2)

### Author contributions

Conceptualization, P.O., M.O., J.W.; methodology, W.D., P.M.; software, P.M., D.P.; validation, P.M.; formal analysis, W.D., P.M.; investigation, P.O., M.O., J.W.; resources, P.M., J.W.; data curation, P.O., M.O., J.W.; writing—original draft preparation, P.O., M.O., J.W.; writing—review and editing, P.M., D.P.; visualization, P.O., M.O., D.P., J.W.; supervision, W.D., P.M.; project administration, P.M.; funding acquisition, P.M. All authors have read and agreed to the published version of the manuscript.

### Declarations

#### Competing interests

The authors declare no competing interests.

#### Additional information

**Correspondence** and requests for materials should be addressed to J.W.

**Reprints and permissions information** is available at [www.nature.com/reprints](http://www.nature.com/reprints).

**Publisher's note** Springer Nature remains neutral with regard to jurisdictional claims in published maps and institutional affiliations.

**Open Access** This article is licensed under a Creative Commons Attribution-NonCommercial-NoDerivatives 4.0 International License, which permits any non-commercial use, sharing, distribution and reproduction in any medium or format, as long as you give appropriate credit to the original author(s) and the source, provide a link to the Creative Commons licence, and indicate if you modified the licensed material. You do not have permission under this licence to share adapted material derived from this article or parts of it. The images or other third party material in this article are included in the article's Creative Commons licence, unless indicated otherwise in a credit line to the material. If material is not included in the article's Creative Commons licence and your intended use is not permitted by statutory regulation or exceeds the permitted use, you will need to obtain permission directly from the copyright holder. To view a copy of this licence, visit <http://creativecommons.org/licenses/by-nc-nd/4.0/>.

© The Author(s) 2025